



Universiteit  
Leiden  
The Netherlands

## Chaotic Dynamics in N-body systems

Boekholt, T.C.N.

### Citation

Boekholt, T. C. N. (2015, November 10). *Chaotic Dynamics in N-body systems*. Retrieved from <https://hdl.handle.net/1887/36077>

Version: Not Applicable (or Unknown)

License: [Licence agreement concerning inclusion of doctoral thesis in the Institutional Repository of the University of Leiden](#)

Downloaded from: <https://hdl.handle.net/1887/36077>

**Note:** To cite this publication please use the final published version (if applicable).

Cover Page



Universiteit Leiden



The handle <http://hdl.handle.net/1887/36077> holds various files of this Leiden University dissertation

**Author:** Boekholt, Tjarda

**Title:** Chaotic dynamics in N-body systems

**Issue Date:** 2015-11-10

# 6

---

## Event-driven Chaos in Dynamical Systems

Based on: *Event-driven Chaos in Dynamical Systems* by T. C. N. Boekholt,  
F. I. Pelupessy, D. C. Heggie and S. F. Portegies Zwart in preparation

In 1207BC, a year after Odysseus returned to Ithaca, the comet P1/Halley should have been visible from the Ionian islands, but apparently was not sighted (?). Since then the short-period comet P1/Halley has intrigued astronomers, policy makers (?), religious leaders (??), artists and the general public for its splendour.

More recently, Halley gained considerable interest because of its importance for understanding the stability of the solar system. The comet probably migrated towards its current orbit in the last 200,000 years (?). Small variations in its time of sighting over the last millennium have prompted astronomers to the possible chaotic nature of the comet's orbit (?). In particular the recent discussion of the chaotic nature of its orbit, as derived by ? requires us to revisit the chaotic nature of Halley's orbit, the origin of its chaos and its short Liapounov time.

We construct a general model for the growth of perturbations in a few-body dynamical system. Using a map to describe the time evolution of the orbital frequency of Halley's orbit, we find that a sequence of close encounters with Jupiter causes exponential growth with a Liapounov time of order 300 years. This short Liapounov time is a natural consequence of the density of close encounters and the strength of each encounter. Numerical integrations however, show that Venus is currently the dominant source of chaos in Halley's orbit.

### 6.1 INTRODUCTION

Whether a dynamical system, such as a planetary system, a star cluster or a galaxy, is stable or unstable is an important property of the system. For example, from an observational point of view, it tells us

about the likelihood to observe a system in a certain state. If the configuration is unstable, it will evolve to a different configuration on a relatively short time scale, so that statistically, it is unlikely to be observed. From a numerical perspective, the stability tells us about the time scale on which we can accurately predict the orbits of the constituent bodies. For a chaotic system, initially nearby solutions will quickly diverge away from each other, resulting in very different outcomes (????).

The stability of a configuration is determined by perturbing the configuration and calculating how the perturbation grows in time. If this growth follows a power law, the system is considered regular. Examples of regular dynamical systems are two-body (point-particle) binary stars, strictly hierarchical triples (e.g. ?) and the three-body figure-8 orbit (??). If the growth instead is exponential, then the system is considered to be chaotic. Examples of chaotic three-body problems are the Pythagorean problem (??), the equilateral triangle (e.g. ?) and the Sitnikov problem (e.g. ?).

Chaos in larger systems was investigated by ?. For time scales shorter than a million years, the divergence of the planets in our solar system closely resembles a power law. At later times however, it turns out that the divergence is really an exponential with an e-folding time of about 5 Myr (?). The time over which the stability has to be determined is thus an important factor.

It is also possible for a system to evolve from order to chaos and vice versa. In a different study of the solar system ? reproduced the exponential divergence found by ?. After  $\sim 50$  Myr however, they observed a transition to a faster exponential growth (?, Fig. 1). The origin of this transition is not known. It might be physical and related to a different chaoticity for the terrestrial and Jovian planets. A numerical artefact is however not excluded.

A more intuitive example of a transition can be constructed for a three-body system consisting of a binary star and a single star that is relatively far but still bound, moving towards the binary star. Since at the start of the experiment the single and the binary star are well separated, the system will behave regularly. At small separations, however, the interplay of the three particles becomes much more irregular, resulting in a prolonged chaotic phase during the resonant encounter (?). In the resonant phase perturbations can grow by orders of magnitude (?).

Dynamical chaos is also present in star clusters, i.e. open clusters and globular clusters. ? measured an exponential growth of perturbations for a small stellar system. ? estimate the e-folding time for

this growth to be on the order of a crossing time, which is the typical time for a star to cross the cluster once. Due to this relatively short time scale, accurate long term integrations of star clusters are virtually impossible. The exponential divergence can be fought using high-precision integrations, but they are prohibitively expensive (?). Transitions in the rate of divergence also occur for star clusters. Starting with a cluster consisting of single stars, close encounters and interactions with a binary star during the moment of core collapse significantly increases the rate of divergence (?, Fig. 3).

Much work has been done to measure the stability of dynamical systems. Less work has been done on the origin of chaos in dynamical systems and transitions in the rate of divergence. ? construct a model for the growth of perturbations in a star cluster. In a somewhat analogous way as in the derivation of the relaxation time of a stellar system (Chandrasekhar, 1942), they relate a linear growth of error to the linear growth in separation after a deflection due to a 2-body encounter (?, Fig 1). A sequence of 2-body encounters can result in the accumulation of power laws, which approximates exponential divergence. This is analogous to a feature already present in a hard-sphere gas (?).

We present a new model for the rate of divergence in few-body dynamical systems, which is based on 2-body Keplerian orbits being perturbed by a third body. Using the fact that a 2-body Keplerian system shows linear divergence and that the accumulation of power laws can produce exponential growth, we are able to model both regular, chaotic and transitional behaviour. We explain the model in more detail in Sec. 6.2.

Next we turn to the case of Halley's Comet (hereafter just Halley), which is perturbed by the planets. Its chaoticity has been verified in several studies (e.g. ?????). The e-folding time for the exponential divergence has been determined to be on the order of the orbital period of Halley or less ( $< 76$  years). One of the aims of this study is to understand the origin of this short time scale. To this end, in Sec. 6.3 we define a map similar to those in ? and ?, which uses kick-functions to model the perturbations due to the planets on Halley. Using this map we investigate the onset of exponential growth of perturbations. In Sec. 6.4 we measure the rate of divergence between neighbouring solutions using precise N-body integrations of the orbit of Halley in the solar system. We compare the data to our semi-analytical model to gain a better understanding of the origin of chaos, the cause of its short e-folding time scale, i.e. the Liapounov time, and the physical mechanism responsible for transitions in the rate of divergence.

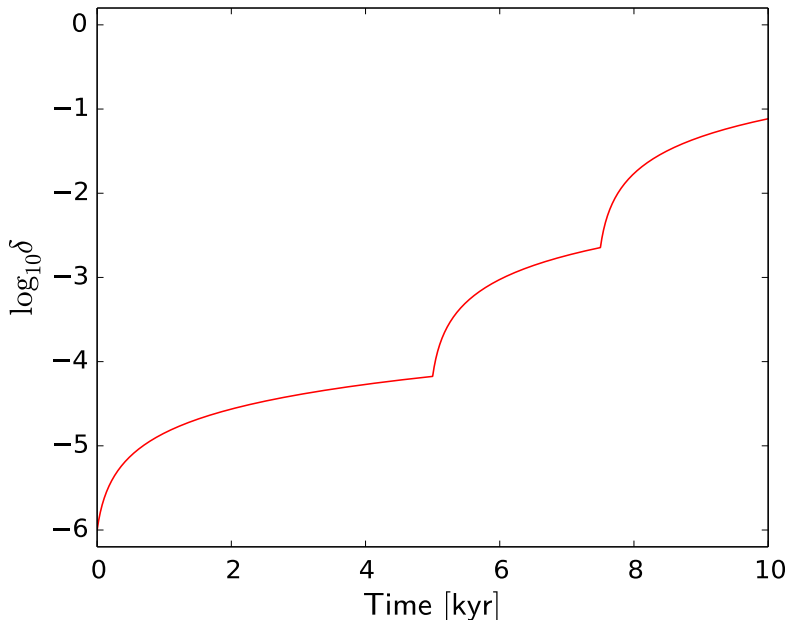


Figure 6.1: Growth of displacement between neighbouring solutions during two scattering events. The diagram, which is intended to be schematic, was plotted using eqs.(6.1), (6.3) and (6.4) for  $\delta_0 = 10^{-6}$ , a constant period  $P = 76$  years,  $f = 1/P$  and encounter times  $t_1 = 5000$  and  $t_2 = 7500$  years.

## 6.2 EVENT-DRIVEN CHAOS

Consider Kepler motion with initial semi-major axis  $a_0$ , total mass  $m$  and initial frequency  $f_0 = \sqrt{m/a_0^3}$  (gravitational constant  $G = 1$ ). Let a neighbouring solution be separated by a small displacement  $\delta_0$  initially. (For simplicity we also suppose that the difference in velocity is small.) This displacement has components along and transverse to the orbit, and we assume that they are both of equal magnitude. The cross-orbit component gives rise to a difference in semi-major axis of the same order, i.e.  $\Delta a_0 \sim \delta_0$ . The resulting difference in frequency is  $\Delta f_0 \sim \delta_0 \sqrt{m/a_0^5}$ . By time  $t > 0$  the displacement along the orbit will have grown to an amount of order

$$\delta(t) \sim \delta_0 + a_0 \Delta f_0 t \sim \delta_0 (1 + f_0 t). \quad (6.1)$$

This growth is linear in  $t$ , but the growth in  $\delta$  from  $t_0$  to  $t$  leads to no growth in  $\Delta a$ , because the growth is along the direction of orbital motion.

Now suppose a short-lived significant perturbation acts on the motion at time  $t_1$ , and that the velocity of the Kepler motion changes direction significantly. The displacement  $\delta_1$  at that time now does have a significant component which is not along the new direction of orbital motion. Thus the variation in semi-major axis is now

$$\Delta a_1 \sim \delta_1, \quad (6.2)$$

and this leads to a difference in orbital frequency  $\Delta f_1 \sim \Delta a_1 f_1 / a_1$  at time  $t_1$ . Thus for  $t > t_1$ , the displacement varies as

$$\delta(t) \sim \delta_1 + \Delta a_1 f_1 (t - t_1) \sim \delta_1 (1 + f_1 (t - t_1)). \quad (6.3)$$

This is again a linear growth, but with a different frequency and initial perturbation. If a second strong perturbation occurs at time  $t_2 > t_1$ , we can see from eqs.(6.1) and (6.3) that the displacement is

$$\delta_2 \sim \delta_0 (1 + f_0 t_1) (1 + f_1 (t_2 - t_1)), \quad (6.4)$$

with a subsequent growth of similar form as Eq. 6.3. A schematic plot of eqs.(6.1), (6.3) and (6.4) is given in Fig.6.1. The result qualitatively resembles the numerical result of ?, Fig. 3. The main difference is that their numerical result has a regular oscillation superposed on the trend illustrated, because the motion in the numerical example is eccentric.

If the perturbations recur at roughly comparable intervals  $\Delta t$ , and if  $f$  does not change by a large factor, it can be seen that the displacement at some large time  $t$  will be

$$\delta(t) \sim \delta_0 (1 + f \Delta t)^{t/\Delta t}. \quad (6.5)$$

In this way we see that the linear growth of Eq.(6.1) transforms into exponential growth, and can easily estimate that the corresponding Liapounov exponent is of order  $f$  if  $f \Delta t \lesssim 1$ . This means it is of order the reciprocal of the crossing time. The case  $f \Delta t \gtrsim 1$  is also of interest, and leads to a smaller estimate of order  $\ln(f \Delta t) / \Delta t$ .

Up to a point we can think of a resonant three-body scattering event as a prolonged sequence of perturbations of Kepler motion. As long as the three bodies remain at comparable distances and are of comparable mass the perturbations in any of the three two-body motions will be of order 1 and will take place at intervals of order the crossing time. Therefore, in accordance with the above discussion, the Liapounov exponent will be of order  $1/t_{cr}$ , with  $t_{cr}$  the crossing time.

Indeed the numerical examples of ? show that the separation of neighbouring solutions grows roughly exponentially until dissolution of

the resonance. The lifetime of the Pythagorean problem, for example, is about 16 crossing times (Aarseth, 2003, p. 238), and the growth of the separation of neighbouring solutions in this time is about 8.5 dex (?). Thus the finite-time Liapounov exponent is of order  $1/t_{cr}$ .

If the evolution of the triple system is dominated by protracted excursions of the third body, of order  $T \gg t_{cr}$ , then the estimate will decrease to one of order  $1/T$  (in accordance with the result for the case  $f\Delta t \gtrsim 1$ , and neglecting a logarithm). Usually, the evolution is a mix of prolonged excursions interspersed with periods of frequent interplay (Szebehely, 1972), and the Liapounov exponent,  $\lambda$ , will be intermediate between limits  $1/T \lesssim \lambda \lesssim 1/t_{cr}$ , where  $T$  is the duration of the longest excursion.

The model we have used neglects the fact that there are, even in the two-dimensional problem we have discussed, four components of the deviation to take into consideration, i.e. two in configuration space and two in velocity space. But the only one of these which can grow secularly (between perturbations) is the component of  $\delta$  along the orbit, and its growth is accounted for approximately in our model.

The result of the model (that the Liapounov exponent  $\lambda$  is of order  $1/t_{cr}$  for comparable masses) is consistent with the results in ?, who considered the general N-body problem. This is rather independent confirmation, as their model was based on assuming that the deviation between neighbouring solutions grows as a result of two-body encounters.

### 6.2.1 Generalization

The secular growth of a perturbation in a two-body system is proportional to the difference in orbital frequency,  $\Delta f$ , between the two neighbouring solutions. Due to events such as close encounters (or other events such as moments of significant mass loss (?)), the difference in orbital frequency will generally be a function of time,  $\Delta f(t)$ . Every time  $\Delta f$  changes, the subsequent growth of the perturbation is linear, proportional to the new value of  $\Delta f$ . In general we can write

$$\delta(t) \sim \delta_0 + \int_0^t \Delta f(T) dT. \quad (6.6)$$

If  $\Delta f(t)$  is a constant,  $\Delta f$ , we obtain Eq. (6.1) for linear growth of the perturbation. Other types of behaviour are also possible. For example, if  $\Delta f$  keeps flipping sign, e.g.  $\Delta f(t) \sim \sin(t)$ , the integral will be zero on average and we obtain no secular growth of perturbations.

Exponential growth of perturbations is obtained if  $\Delta f(t)$  grows exponentially. As described in Sec. 6.2, this can be obtained if there is a regular sequence of close encounters, e.g. changes in  $\Delta f$ . We can estimate a finite-time Liapounov exponent by equating Eq. (6.6) to an exponential with Liapounov exponent  $\lambda$ , resulting in

$$\lambda(t) = \frac{1}{t} \ln \left( 1 + \frac{C}{\delta_0} \int_0^t \Delta f(T) dT \right). \quad (6.7)$$

Here  $C$  is a constant depending on the configuration and this approximate expression will approach the Liapounov exponent at large  $t$ .

### 6.3 THE ONSET OF EXPONENTIAL DIVERGENCE

In the previous section we have shown that an event, such as a close encounter with a third body, can cause the rate of divergence between two neighbouring solutions to increase. The growth of an initially small perturbation is thus related to the encounter history of the binary with a third body. In this section we measure the growth of perturbations using a map similar to those of ? and ?, with a kick function to model the effect of encounters. The model is particularly adapted to a case like that of Comet Halley, in which the masses of the perturbers are small, unlike the case of comparable masses considered in Sec.2.

#### 6.3.1 Map for Changes in Orbital Frequency

We are interested in the time evolution of the difference in orbital frequency,  $\Delta f$ , since this quantity drives the growth of perturbations. We consider a system similar to the three-body system consisting of the sun, Jupiter and Comet Halley. Each orbital period Halley will encounter Jupiter at a certain distance,  $R$ , depending on the orbital phase of Jupiter,  $\phi$ . We define the kick function  $K(\phi)$  to be the  $2\pi$ -periodic function that gives the change in orbital frequency  $\delta f$  as a function of  $\phi$ . Depending on the geometry of the configuration, different kick functions are possible. A sawtooth-like function is appropriate for the configuration under discussion (??).

The map is given by

$$\phi_{n+1} = \phi_n + 2\pi \left( \frac{f_J}{f_n} \right) \quad (6.8)$$

$$f_{n+1} = f_n + K(\phi_{n+1}), \quad (6.9)$$

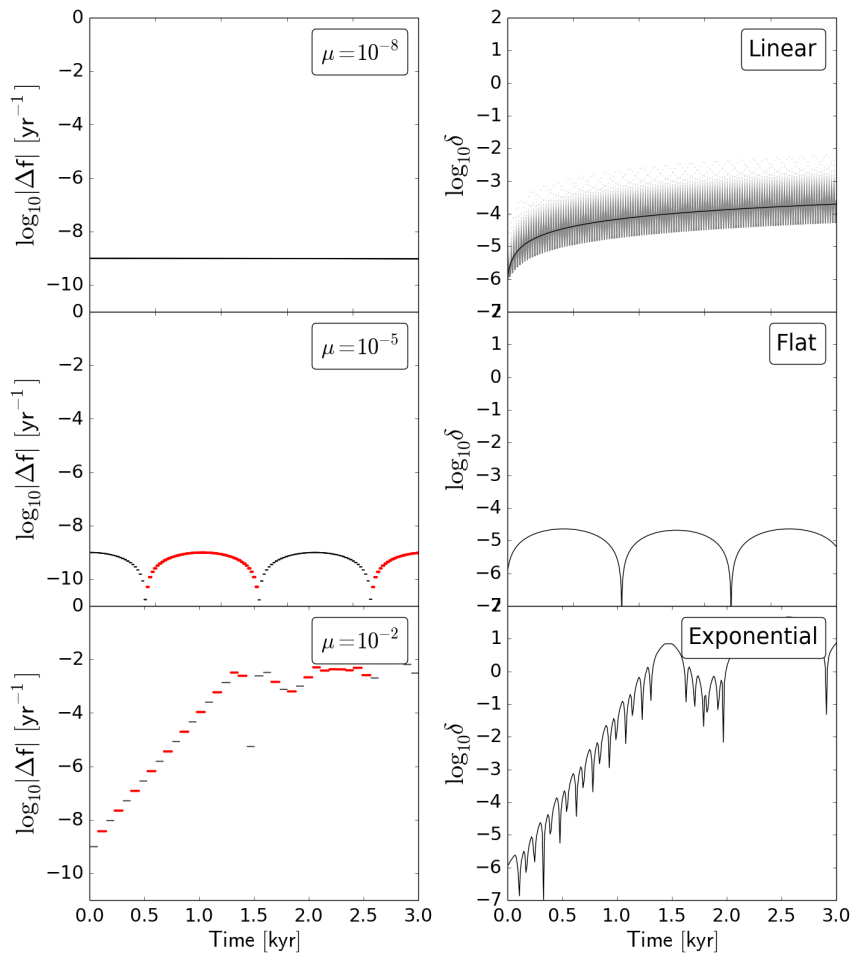


Figure 6.2: Illustration of the three types of behaviour for the growth of perturbations. The time evolution of the difference in orbital frequency  $\Delta f$  between two neighbouring solutions (left column) and the consequent growth or perturbation (right column), are presented for three different encounter strengths  $\mu = 10^{-8}$ ,  $10^{-5}$  and  $10^{-2}$ . In the left column, the data is represented by a thin line if  $\Delta f > 0$  and fat otherwise.

where  $\phi_n$  is the phase (i.e. longitude) of Jupiter at the  $n$ th perihelion passage,  $f_n$  is the frequency of Halley after the  $n$ th perihelion passage, and  $f_J$  is the (constant) frequency of Jupiter. The times can be obtained recursively from

$$t_{n+1} = t_n + \frac{1}{f_n}. \quad (6.10)$$

Time is measured in years,  $f$  in  $\text{yr}^{-1}$  and semi-major axis, when we need it, in AU. The orbital periods of Halley and Jupiter are given by  $P_h \simeq 75.3$  yr and  $P_J \simeq 11.9$  yr respectively, and we use these values to compute the exact starting value  $f_0 = 1/P_h$ , and the value of  $f_J$ . Note that they are approximately in a 3:19 resonance.

To study the separation of neighbouring solutions we construct the tangent map, i.e. the linearisation of the above map, given by

$$\Delta\phi_{n+1} = \Delta\phi_n - 2\pi \frac{f_J}{f_n^2} \Delta f_n \quad (6.11)$$

$$\Delta f_{n+1} = \Delta f_n + \Delta\phi_{n+1} K'(\phi_{n+1}). \quad (6.12)$$

We see from eqs.(6.11), (6.12) that the change in  $\Delta\phi$  is a negative multiple of  $\Delta f$ , whereas if  $K' > 0$  the change in  $\Delta f$  is a positive multiple of  $\Delta\phi$ . This interplay causes interesting behaviour as we will illustrate in Sec.6.3.2 below.

When the right side of Eq.(6.12) is expressed in terms of  $\Delta\phi_n$  and  $\Delta f_n$ , it takes the form

$$\Delta f_{n+1} = \Delta f_n + \left( \Delta\phi_n - 2\pi \frac{f_J}{f_n^2} \Delta f_n \right) K'(\phi_{n+1}). \quad (6.13)$$

Combining with Eq.(6.11), we see that the matrix of the linearised map is given by

$$A = \begin{pmatrix} 1 & -2\pi \frac{f_J}{f_n^2} \\ K'(\phi_{n+1}) & 1 - 2\pi \frac{f_J}{f_n^2} K'(\phi_{n+1}) \end{pmatrix}. \quad (6.14)$$

This matrix has determinant one, showing that our map is *symplectic* (i.e. area-preserving). Thus although the variables  $f, \phi$  are not canonical in the usual sense (energy and phase would be better), the map preserves the main geometrical constraint of a canonical mapping. The eigenvalues of  $A$ , which will be useful below, are

$$\lambda = 1 - \pi \frac{f_J}{f_n^2} K' \pm \sqrt{\pi \frac{f_J}{f_n^2} K' \left( \pi \frac{f_J}{f_n^2} K' - 2 \right)}, \quad (6.15)$$

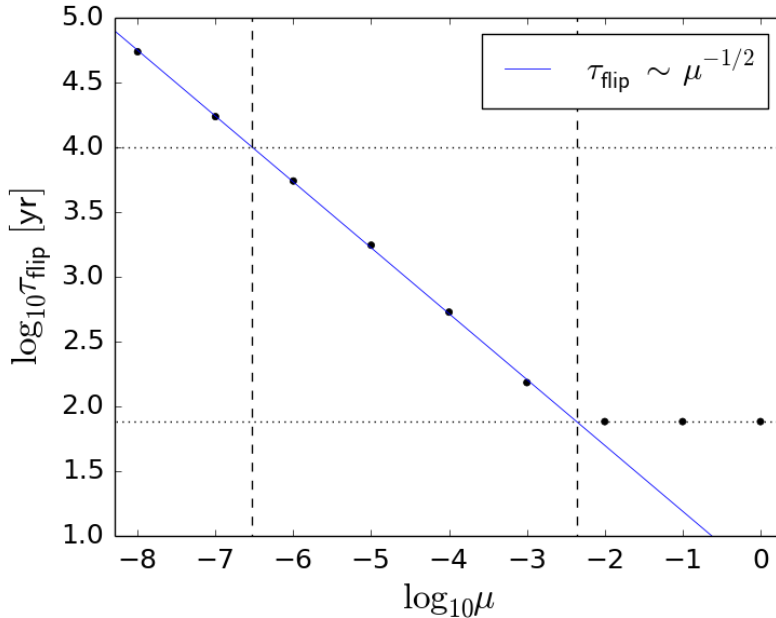


Figure 6.3: The time until the first change of sign,  $\tau_{flip}$ , as a function of the strength of the perturbation,  $\mu$ . The top dotted line marks the 10 kyr time of interest, whereas the bottom dotted line marks the orbital period of Halley. Exponential divergence occurs when  $\tau_{flip}$  is smaller than the orbital period.

where  $K' = K'(\phi_{n+1})$ .

For numerical purposes we sometimes measure the difference between two solutions by a formula adapted from Eq.(6.6), whose right side can be computed from

$$\delta_{n+1} = \delta_n + C\Delta f_n \frac{1}{f_n}. \quad (6.16)$$

Another technicality of these numerical calculations is that  $\phi_n$  and  $\Delta\phi_n$  are stored mod  $2\pi$ .

### 6.3.2 Linear Kick Function

We first consider the idealised case in which the kick function is the  $2\pi$ -periodic function defined by the relation

$$K(\phi) = \frac{\mu}{2\pi}\phi \quad \text{on } [0, 2\pi) \quad (6.17)$$

with  $\mu$  a free parameter. Note that the derivative of the kick function is a constant (except at the discontinuity when  $\phi$  is an integral multiple of  $2\pi$ ). In this model every kick has the same contribution to the growth of perturbation in the orbital frequency. This is approximately the case when there is a regular sequence of similar encounters, i.e.  $\phi_n$  is almost independent of  $n$ , mod  $2\pi$ .

We start with the initial values  $t = 0$ ,  $\phi = 0$ ,  $\Delta\phi = 0$  and  $\Delta f = 10^{-9}$  (which corresponds to a  $\Delta a \simeq 10^{-6}$ ). We vary the value of  $\mu = 10^{-8}$ ,  $10^{-5}$  and  $10^{-2}$  to model encounters of different strengths. In Fig. 6.2 we plot the time evolution of  $\Delta f$  (top row) and the consequent growth of perturbation (bottom row) through Eqs. (6.8)–(6.16).

For the weakest perturbations no variation in  $\Delta f$  is detectable on the scale of the plot, thus we get a linear growth of the perturbation. The data points which are also plotted in this panel (bottom left) are data from a numerical simulation where we integrated the orbit of Halley around the sun without perturbers. A good fit is obtained for a proportionality constant  $C = 20$  (see Eq. 6.7). Although this value has no particular significance, it gives an impression of how the simple model we are considering may apply to Halley, and we use it in the remainder of this study.

If we make the perturbations somewhat stronger (Fig. 6.2 central panels) we observe an oscillatory behaviour such that the perturbation in  $\Delta f$  never exceeds its initial value but alternates in sign. To understand this oscillatory behaviour better, we compute the eigenvalues of the matrix  $A$ . From eqs.(6.15) and (6.17) we readily find that

$$\lambda = 1 - \frac{\mu f_J}{2f_n^2} \pm \sqrt{\frac{\mu f_J}{2f_n^2} \left( \frac{\mu f_J}{2f_n^2} - 2 \right)} \quad (6.18)$$

$$\simeq 1 \pm i \sqrt{\frac{\mu f_J}{f_n^2}} \quad (6.19)$$

when  $|\mu| \ll 1$ . This shows that the evolution is expected to be oscillatory (if  $\mu > 0$ ), and the period (in years) is given approximately by

$$P = \frac{2\pi}{\sqrt{\mu f_J}}, \quad (6.20)$$

which gives a value of 6854 yr for  $\mu = 1 \times 10^{-5}$ , i.e. very consistent with what would be inferred from Fig.6.2 (middle column).

For the strongest perturbation (Fig. 6.2 right panels) we observe exponential growth of perturbations. This growth saturates at  $\log_{10} \delta \sim$

0 since the growth is limited by  $\Delta\phi < 2\pi$ . In other words, the perturbation has grown to the size of the system. We observe again the sign flipping of  $\Delta f$ , however this time it occurs after every orbital period. The exponential growth is explained again by Eq.(6.18), which shows that the eigenvalues  $\lambda$  are real if

$$\mu > \frac{4f_n^2}{f_J} = \frac{4P_J}{P_h^2} \simeq 0.0084. \quad (6.21)$$

Also, their product is unity, and so one eigenvalue has magnitude  $|\lambda| > 1$ , resulting in exponential growth.

To understand the relation between the period of the oscillatory behaviour and the secular growth of perturbations in more detail, we plot in Fig. 6.3 the time to the first change of sign. (Note that this will be  $0.25P$ , in the notation of Eq.(6.21), as it is evident from Fig.6.2, central column, that the oscillation starts at maximum.) First, we observe that towards increasing values of  $\mu$ , the flip time scale decreases as  $\tau_{flip} \sim \mu^{-1/2}$ , as predicted in Eq.(6.20). To the left of the vertical, dashed line at  $\log_{10} \mu \sim -6.5$ , the period is longer than 10 kyr, so that on such a time scale we observe a constant  $\Delta f$  and a linear growth of perturbation. In between the two vertical dashed lines we observe oscillatory behaviour with decreasing period. A transition in the behaviour occurs once the period is of the order the orbital period of Halley (marked by vertical dashed line at  $\log_{10} \mu \simeq -2.4$ ). The critical value of  $\mu \simeq 0.004$  and for larger values we obtain exponential growth of perturbations. The theoretical prediction that exponential growth occurs for  $\mu \gtrsim 0.0084$ , i.e.  $\log_{10} \mu \gtrsim -2.08$ , is consistent with the numerical data plotted in Figs. 6.2 and 6.3.

### 6.3.3 Saw-tooth Kick Function

In a more realistic kick function there will be both weak and strong encounters present. We use the following derivative of the kick function

$$\frac{dK(\phi)}{d\phi} = \frac{\mu_{max}}{2\pi}, \phi < \phi_c, \quad (6.22)$$

$$\frac{dK(\phi)}{d\phi} = \frac{\mu_{min}}{2\pi}, \phi \geq \phi_c. \quad (6.23)$$

To investigate transitions in the rate of divergence we take our map from Sec. 6.3.1, and vary the free parameters in the kick function ( $\mu_{max}, \mu_{min}$ ) as follows:  $(10^{-2}, 10^{-5})$ ,  $(10^{-2}, 10^{-8})$  and  $(10^{-5}, 10^{-8})$ . These pairs of values correspond to the different regimes of behaviour

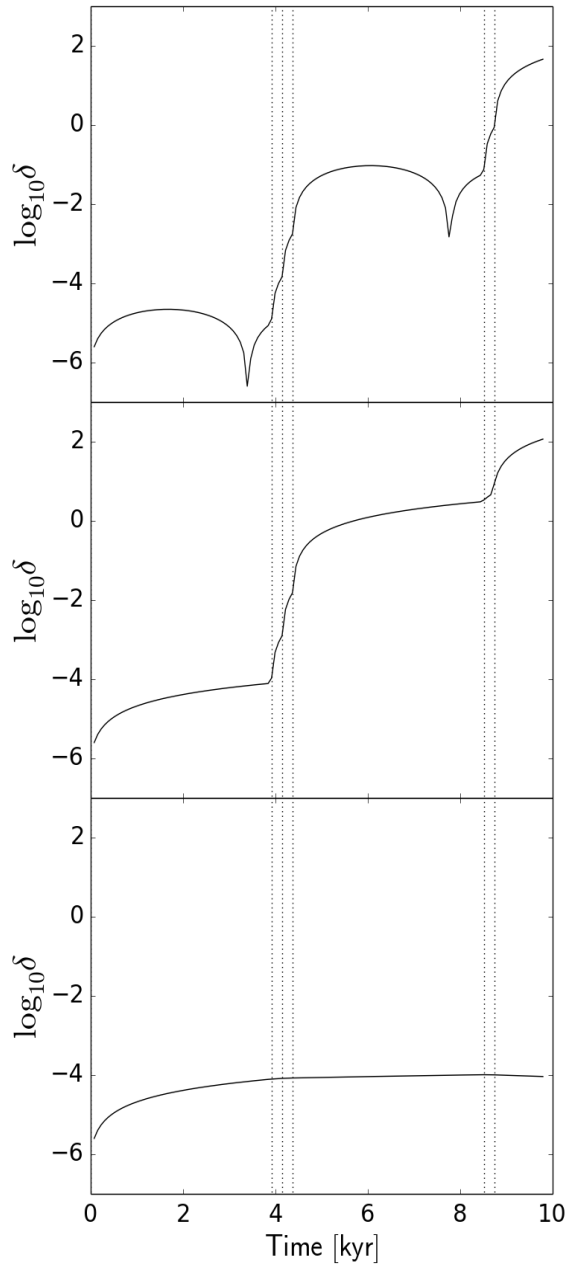


Figure 6.4: Transitions in the rate of divergence as a consequence of the close encounter history between Halley and Jupiter. The close encounter times are marked by the vertical dotted lines. The panels illustrate different types of transitions: oscillatory to exponential (top), linear to exponential (middle) and linear to oscillatory (bottom).

(see Fig. 6.3). We create a small window for the strong perturbations to occur by setting  $\phi_c \sim 0.3$ , which corresponds to a periodic sequence of roughly two or three strong encounters<sup>1</sup>. We illustrate the results belonging to the encounter history given by  $\phi_0 = 0$  in Fig. 6.4. The close encounter events are marked by the vertical, dotted lines.

In the left panel, the growth of the perturbation starts out oscillatory ( $\mu = 10^{-5}$ ). After about 4 kyr there is a sequence of three close encounters causing the characteristic accumulation of power laws or “hops” in the divergence as explained in Sec. 6.2. Once these encounters are over however, the growth becomes oscillatory again.

In the central panel of Fig. 6.4 we observe a similar behaviour, but instead of the oscillatory behaviour we have a linear growth since  $\mu = 10^{-8}$  in those intervals. It is clear from these examples that these transitions are caused by a sequence of close encounters. Finally, in the right panel we observe a transition from power law to oscillatory divergence which effectively produces no secular growth.

### 6.3.4 Liapounov Time

A characteristic time scale for divergence is somewhat difficult to determine for a solution showing transitional behaviour. Once a solution does diverge exponentially it does so with a rate that depends on the strength of the perturbation and the density of close encounters.

To estimate a lower limit for the Liapounov time, we set the orbital period of Halley to  $P_h = 76$  yr and that of Jupiter to  $P_J = 12$  yr, so that they are exactly in a 3:19 resonance. Therefore, if Halley once experiences a close encounter with Jupiter, it does so every three orbital periods. We use the saw-tooth kick function with  $\mu_{min} = 10^{-8}$  (linear growth) and we vary  $\mu_{max}$  in the exponential regime to measure the Liapounov time as a function of the strength of the perturbation. We measure  $\Delta f(t)$  using the map from Sec. 6.3.1 and calculate the approximate Liapounov time using Eq. 6.7, evaluated at the moment when the perturbation  $\delta = 1$ . We show the result in Fig. 6.5.

The variation in the Liapounov time decreases as  $\mu$  increases through the critical value corresponding to  $\log_{10} \mu \simeq -2.08$ , i.e. the transition from periodic behaviour to exponential growth (dashed, green line). From values exceeding a thousand years it quickly drops to a value of the order the orbital period of Halley (blue, horizontal line). Very

---

<sup>1</sup>There is a small drift in the orbital phase because Halley and Jupiter are not exactly in a 3:19 resonance. In fact  $3P_h - 19P_J = 0.2\text{yr}$  if  $P_h = 75.3\text{yr}$  and  $P_J = 11.9\text{yr}$ . It is then easy to see that these sequences of close encounters recur at intervals of about 4.5kyr.

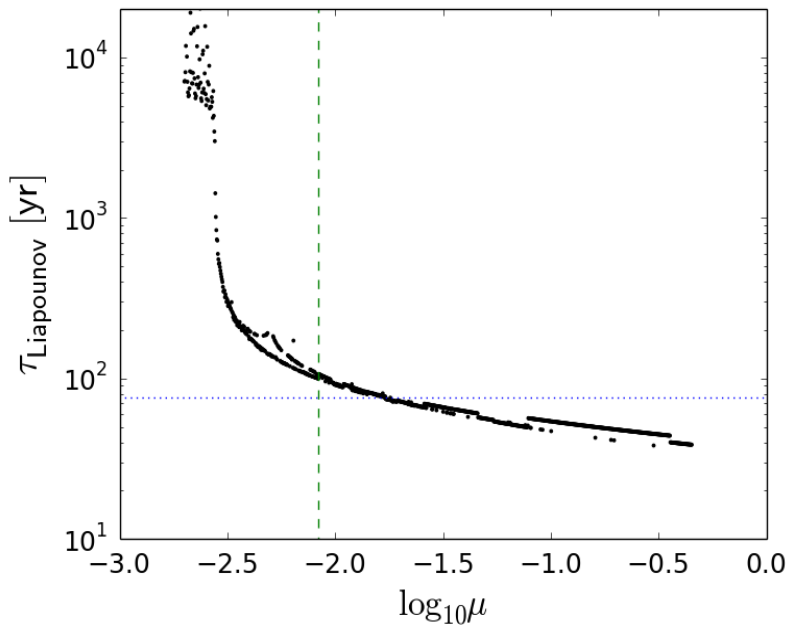


Figure 6.5: Estimated Liapounov time as a function of encounter strength, for a configuration where Jupiter and Halley are in a 3:19 mean motion resonance. The horizontal dotted line gives the orbital period of Halley, and the vertical dashed line marks the critical value of  $\mu$  as derived in Eq. 6.21.

strong perturbations decrease the Liapounov time to values as low as 30–40 yr. What intuitively seemed like a very short time scale for the exponential growth, actually follows naturally from the recurrence of close encounters in time and the strength of each perturbation. The saturation at low values of  $\mu$  is due to the finite integration time, whereas the small scatter along the curve is due to errors in calculating the Liapounov time from Eq. 6.7 and the slight variation in the final value of  $\delta < 1$ .

It must be stressed that these estimates of the Liapounov time are based on the artificial imposition of a resonance ensuring that close encounters recur at every third perihelion passage, i.e. every 228yr. Their frequent recurrence will also ensure that  $f$  changes, throwing the system out of resonance and increasing the Liapounov time. For example, in the situation shown in Fig.6.4, corresponding to the present-day periods, close encounters recur on average once every 1.5kyr. Furthermore we have focused on the case in which  $\mu > 0$ . In case  $\mu < 0$  we can see from Eq.(6.18) that the eigenvalues of  $A$  are always real, giving exponential growth. When  $-1 \ll \mu < 0$ , the Liapounov time can be estimated from

$$T_{Liapounov} \simeq \frac{1}{\sqrt{-\mu f_j}}. \quad (6.24)$$

In reality, the kick function  $K(\phi)$  is approximately a saw-tooth function, as we have been assuming, but there is a significant difference. Since it is a periodic function, its derivative cannot always be positive. Indeed, as shown by ?<sup>2</sup>  $K(\phi)$  (the kick due to Jupiter) is an increasing function of  $\phi$ , except for a small range of  $\phi$  in which  $K' < 0$ . Thus  $K$  resembles the function considered in this section, except that  $\mu_{max} < 0$ . (The “max” may be taken to refer to the magnitude of  $\mu$ .) It therefore seems likely that most encounters are of what we have called the oscillatory type, while there is a minority in which the behaviour is of exponential type.

#### 6.4 N-BODY SIMULATIONS OF HALLEY’S ORBIT

In this section we describe several experiments in which we perform a series of N-body simulations to measure the growth of an initial perturbation in Halley’s orbit. We model the dynamical evolution of the solar system according to Newtonian dynamics, in which the bodies

---

<sup>2</sup>Their kick function  $F$  is defined as the change in twice the binding energy of Halley, and the binding energy is an increasing function of  $f$ . Therefore  $F$  and  $K$  have the same sign for a given phase.

are mathematical point-particles. Non-gravitational effects, such as radiation pressure from the sun, Halley's mass loss due to the interaction with the stellar wind or internal processes, are neglected. This makes our results less realistic, but for our study on the origin of chaos in Halley's orbit, the gravitational interaction with the sun and planets is sufficient. Relativistic effects, especially the orbital precession of Mercury, will also be neglected. Its influence might become important were it to be shown that Mercury affects the chaoticity of Halley in the Newtonian limit.

We use the N-body code Brutus (?), that solves the N-body problem to a pre-defined precision. To make sure that numerical errors do not bias our results, we vary the precision until convergence as described in ?.

The dominant force in Halley's motion is the sun. Small perturbations are superposed due to the interactions with the planets. solar system bodies smaller than the planets are unlikely to be the cause of chaos in Halley's orbit. We therefore only consider the sun, the eight planets and Halley in our N-body simulations. We obtain the initial conditions from the JPL Horizons database <sup>3</sup>.

The orbital elements of Halley are known to about six decimal places (?). Two initial realizations which differ within the observational uncertainty are both equally valid representations of the system. When we measure the growth of perturbations, we will use the fiducial initial realization and compare it to a perturbed initial realization in which a single coordinate (usually the x-coordinate of Halley) is perturbed by  $10^{-6}$  AU (similar as in ?).

#### 6.4.1 Phase Space Distance

A wide variety of methods are available to measure the rate of divergence for a particular orbit (e.g. variational equations (?)) or finite-time Liapounov exponent (e.g. ?). We adopt a simple, direct approach. We take a fiducial initial condition for a certain system of bodies. This initial condition is integrated with a pre-determined precision until the end time. We also take the perturbed initial condition, where we translate the position of Halley along the x-direction by the observational uncertainty  $10^{-6}$  AU. This new initial realization is also integrated with the same precision, until the end time. The phase space distance as a function of time between these two solutions is calculated similar as in ?

---

<sup>3</sup><http://ssd.jpl.nasa.gov/>, JDCT = 2456934.5 = A.D. 2014-Oct-04 00:00:00.0000 (CT)

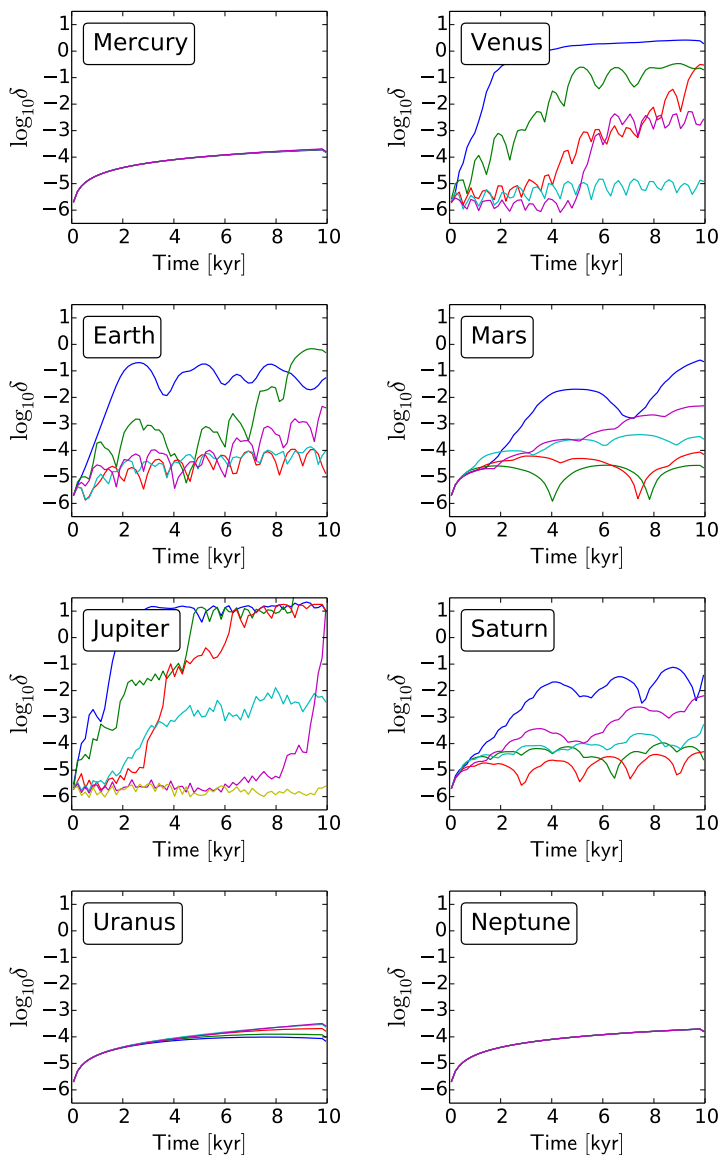


Figure 6.6: Divergence between neighbouring solutions in the  $N = 3$  sun, planet and Halley system. We show a subset of solutions to illustrate the different behaviour when we vary the initial orbital phase of the planet around the sun. As a consequence, every solution has a different encounter history with that planet. Mercury, Uranus and Neptune do not influence Halley’s chaoticity significantly. The other planets are able to cause exponential growth, most notably Jupiter and Venus.

$$\delta_{A,B}^2 = \sum_{i=1}^N \sum_{j=1}^6 (q_{A,i,j} - q_{B,i,j})^2. \quad (6.25)$$

Here  $q$  denotes the phase space coordinate for solutions  $A$  and  $B$ . The sums are over all particles and their phase space coordinates.

If two solutions with the same initial realization are compared, but they were obtained with different precisions, numerical divergence might distort the physical rate of divergence. Therefore, we always compare solutions integrated with the same precision, but with a small, physical perturbation in the initial conditions.

### 6.4.2 Three-body Divergence: sun, planet and Halley

We already showed some results of our simulations in Fig. 6.2 (bottom left panel), where we integrated a two-body system consisting of the sun and Halley. This result confirms the linear growth of perturbations in two-body systems.

We now introduce a perturbing planet to the system. For each planet we generate an ensemble of a thousand initial conditions, where we vary the initial orbital phase of that planet. In every subsequent integration, Halley will experience a different encounter history with the planet, which should produce different rates of divergence as was already illustrated in Sec. 6.3. We show a subset of illustrative cases in Fig. 6.6.

We first observe the results by Jupiter. The rates of divergence vary widely. There are solutions which stay almost constant within a time span of  $10^4$  years (yellow curve). In the other extreme are solutions that grow exponentially and have completely diverged within a few thousand years (blue, green and red curves). In between, there are solutions with different kind of transitions in the divergence. After an initial flat phase of a certain duration, a transition to an exponential growth is possible (red and purple curves), but it is also possible for this exponential growth to convert into a power law divergence (cyan curve).

The influence of Saturn on Halley's stability is less strong, but some solutions still grow exponentially for a few thousand years, after which they make a transition to a power law divergence. The magnitude of the perturbation never really becomes the size of the system. The slope in the exponential part of the blue curve is also shallower than the slope in Jupiter's results. The remaining outer planets show a

power law growth and thus have a negligible contribution to Halley's chaoticity.

The influence of the terrestrial planets varies. Mercury shows regular behaviour irrespective of its encounter history with Halley. It is therefore likely that relativistic effects are unimportant for the chaoticity of Halley's orbit. Venus on the other hand shows a variety of solutions similar to Jupiter. The most rapid growing solution looks similar to the one of Jupiter. The majority of Earth and Mars solutions show a power law divergence superposed with periodic variations. Note however, that they are able to generate a rapid rate of divergence in some situations.

### 6.4.3 Hopping Between Planets

In this experiment we do not randomize the initial orbital phase, but we take the fiducial initial conditions so that we can measure the actual encounter histories of the planets with Halley. We consider the 3-body systems including the sun, a planet and Halley, to measure the independent rates of divergence. Based on the results of Sec. 6.4.2, we neglect Mercury, Uranus and Neptune. We compare these results with a simulation including all the relevant planets collectively. The results are given in Fig. 6.7. We averaged the data over bins of two orbital periods to reduce the short term oscillatory behaviour.

We observe that only Venus (green curve) and Jupiter (yellow curve) produce an exponential divergence. Initially the perturbation due to Venus dominates, but it is overtaken by Jupiter after about 3000 years. The solution including multiple planets (black curve), follows this transition, first following the perturbations due to Venus and then hopping onto the perturbations by Jupiter. Other effects are present since the black curve does not lie perfectly on top of the green and yellow curves. The superposition of independent growth rates is however a reasonable approximation in this example.

From the time evolution of the perturbation in the complete system (black curve) we calculate the average Liapounov time up to the point where  $\delta = 1$  resulting in  $299 \text{ yr} \pm 62 \text{ yr}$ , where the uncertainty is the standard deviation in the variation of the Liapounov time from  $t = 0$  onwards.

To investigate the dependency on the direction of the perturbation, we varied the initial perturbation in Halley's orbit to lie along the x, y or z-direction. We find that in each case Venus is dominant for at least 3000 yr. For the y-direction, Venus remains dominant up to 4000 yr. The rate of divergence due to Venus depends sensitively on Halley's

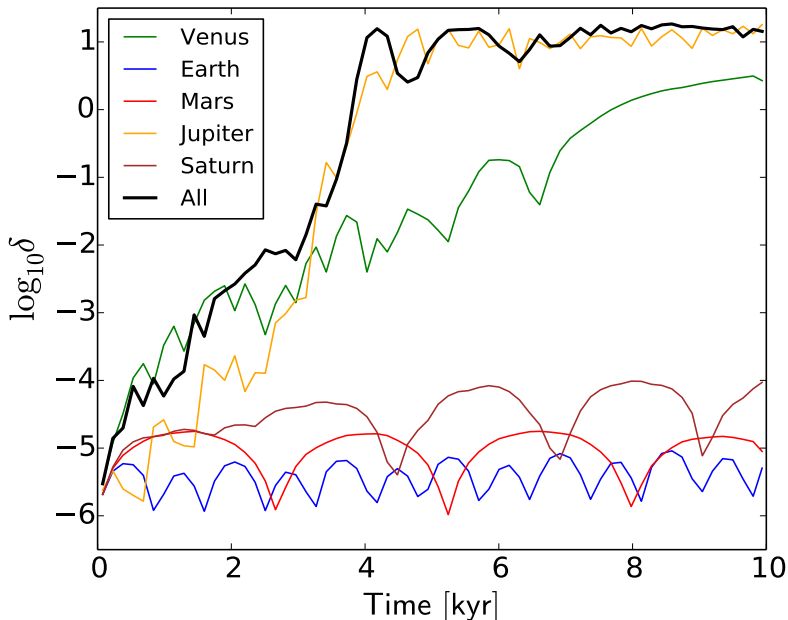


Figure 6.7: Growth of perturbations in time for the different planets independently and with the planets collectively (fat curve). Up to 3000 years, Venus is the dominant perturber of Halley’s orbit. Then a transition occurs and Jupiter becomes the main perturber. The transition in the rate of divergence for the solution including all planets is explained by the superposition of independent rates of divergence of the planets.

orbit. We also performed a similar experiment where we integrated backwards in time. We find that both Venus and Jupiter show an exponential divergence, reaching  $\log_{10} \delta = 1$  after 3 – 4000 yr.

#### 6.4.4 Ensemble Simulations

In the previous section we varied the perturbation in Halley’s orbit along three different directions in space. In this experiment we want to vary the perturbation in all directions in space. Instead of comparing a fiducial and a perturbed solution, we take an ensemble of a hundred Halley-like objects, which are distributed around the fiducial initial position, in a three-dimensional Gaussian distribution with a dispersion of  $10^{-6}$  AU. This eliminates any chance effects of preferred spatial directions. We only consider the perturbations due to the sun and Jupiter. Starting points are the current positions of the sun, Jupiter and Halley. The simulations are done with the Huayno

integrator (?). To study the influence of the strength of the perturbations, we vary the mass of Jupiter by multiplying it by a factor ranging from zero to five. We measure the spread in the positions of the Halley-like objects, i.e. the standard deviation in the position of the ensemble, as a function of time.

We observe in Fig. 6.8 that if the planet has zero mass, we get a linear growth in the dispersion of the positions of the swarm, as expected from the imposed distribution in orbital periods. For small Jupiter masses, i.e. a mass smaller than the actual Jupiter mass, we get a sub-linear growth with an oscillatory behaviour, which we now can understand from our previous analysis to be due to the weak encounter nature of the interactions. Comparing the cases of  $0.2 \times M_{jup}$  and  $0.5 \times M_{jup}$  we see that the mass of Jupiter is of little influence, until there is a strong perturbation, which happens after 9000 yr for half of Jupiter's mass (red curve). The increase in mass versus  $0.2 \times M_{jup}$  remarkably does not increase the growth at all by weak perturbations before that time, it is just increasing the probability of eventually encountering a strong interaction. For heavier Jupiters (i.e.  $1 \times M_{jup}$  and heavier), we obtain a rather fast exponential divergence due to prompt strong interactions.

Note that the experiment conducted here considers the evolution of an ensemble of Halley-like objects, but the results equally apply to a swarm of objects (e.g. the result of an asteroid collision or dust emitted from a cometary nucleus). This means that in configurations where the orbit does not encounter strong interactions, but is affected by weak perturbations such a swarm will survive as a coherent group longer than might be expected from the linear spreading with time.

## 6.5 DISCUSSION AND CONCLUSIONS

### 6.5.1 The Liapounov Time

Previous studies have considered the value of the Liapounov time for the growth of perturbations in Halley's orbit. ? gave an estimate of a lower bound of 34 yr for the Liapounov time, and our estimate is consistent with this. Our estimate is, however, inconsistent with the results of ?, who found a value around 70 yr. This was based on an initial perturbation in the  $y$ -coordinate of Halley, but they also gave results for an initial perturbation in the  $x$ -coordinate (their Fig.7) which would give a Liapounov time only slightly longer. We note, however, that their plot of the growth of the deviation between two orbits (their Fig.6) indicates growth in  $\delta$  (their measure of the separation of two

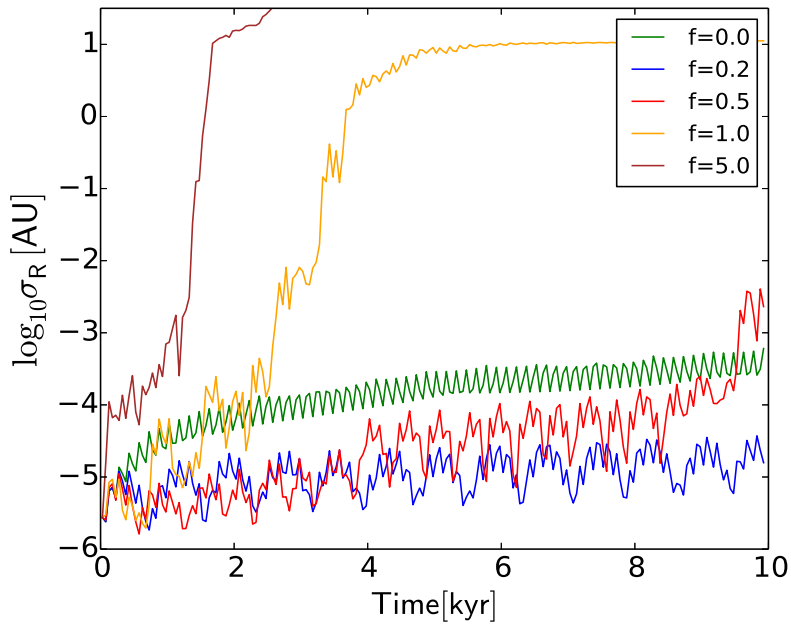


Figure 6.8: Growth of the spread in position of an ensemble of Halley-like objects. We vary the mass of Jupiter by multiplying it by a fraction given in the legend. We reproduce the linear, sub-linear and exponential growth, depending on the strength of the perturbation.

orbits) by about 5 dex in 3.5 kyr, implying a Liapounov time of order 300 years, very similar to ours. Our value for the growth in the separation of two orbits in 3.5 kyr is similar to theirs (see Fig.6.7), and so we suspect an error in their computation of the Liapounov time from correct data.

The Liapounov time of Halley's Comet is determined principally by perturbations due to Venus and Jupiter (Fig.6.6). The influence of Earth, Mars and Saturn is smaller during the next few millennia, and that of Mercury, Uranus and Neptune is negligible. The comparable importance of Jupiter and Venus could not have been guessed from their relative masses. The surprising fact that the mass of a planet does not directly measure its influence on the Liapounov time is illustrated in the very interesting calculations of the kick function (as a function of phase  $\phi$ ) by ?, their Fig.2. That due to Venus has a maximum value about one hundredth of the maximum kick due to Jupiter, which is roughly in proportion to their mass, even though these two planets contribute roughly equally to the Liapounov exponent for Halley. The reason for this is the contribution also depends on the distance of closest approach. This is made apparent by the fact that the divergence caused by these two planets depends strongly on the initial phase (Fig.6.6 again). Indeed ? draw attention to a forthcoming relatively close encounter with Jupiter after about 3.4 kyr, and its influence is visible in Fig.6.7. We drew attention to the importance of a near-resonance in the motions of Halley and Jupiter, and its importance for the growth of divergence between neighbouring orbits (Fig.6.4), and for different planets such configurations will occur at different periods, as the orbits of the system evolve. The importance of Venus to Halley's chaoticity can be explained by noting that Halley crosses the orbital plane of the solar system close to the orbit of Venus.

Much of our focus in Sec.6.3 was on the parameter  $\mu$ , which measures the derivative of our kick function  $K(\phi)$ . This also can be estimated from the results of ?, bearing in mind that their kick function  $F(x)$  is the change (per perihelion passage) in twice the binding energy of Halley, as a function of  $x = \phi/(2\pi)$ . For Venus the largest value of  $|F'|$  occurs over a range of  $x$  of order 0.1 in which  $F$  decreases between values of about  $\pm 0.5 \times 10^{-4}$ . Thus we estimate  $F' \simeq -10^{-3}$ , and infer that  $K' \simeq -10^{-5}$ , though care has to be taken with the different units used in the two studies. This results in  $\mu \simeq -6 \times 10^{-5}$  and so, using Eq.(6.24), we estimate that the corresponding Liapounov time is of order 400 yr. This is of the correct order to account for the most rapid growth in Fig.6.6 (second panel), but it would only occur for phase values within a fairly narrow range. For Jupiter, similar estimates give

a Liapounov time an order of magnitude smaller, again over a similar, limited range of phases. For Venus there is actually another larger range of phase with  $K' < 0$ , but  $|K'|$  is smaller than the estimate we have given, and the Liapounov time correspondingly longer. For both planets the magnitude of  $K'$  is smaller than these upper limits, and so when  $K' > 0$  Halley remains in the regime of oscillatory “growth” (Sec.6.3). When the phases are such that this occurs, it is interesting to note that these perturbations make Halley more stable compared to having no perturbations at all.

Even neglecting the other planets, Venus and Jupiter clearly both contribute strongly to the growth of the divergence between neighbouring orbits. Fig.6.7 illustrates that a sort of superposition principle is approximately valid. It can be seen that the yellow curve for Jupiter alone does not rise quickly immediately, but only after about 2 kyr. The green curve due to Venus gives the opposite behaviour, from a transition from rapid growth to one of slower growth. Meanwhile the black curve (for the entire planetary system) exhibits a transition from the green onto the yellow curve, much as if the two latter effects were superposed. The rate of divergence of the collective system will closely follow that of the most rapidly diverging individual perturbation.

Many factors have been ignored in our work. As shown by ?, Fig. 5, the kick functions are not constant in time. Small variations in the orbital elements alter the maximum value of the derivative of the kick function. The Liapounov time changes in time. In this work the changes in  $\Delta f$  were assumed to be mainly caused by close encounters with a planet. Our model is however more general and other events could cause a change in the orbital frequency as well. For example, Halley lost a significant amount of mass during an event in 1991 (?), the origin of which is unknown. Even though the mass loss will be the same in both neighbouring solutions, the difference in orbital elements will cause the effect of the mass loss event to be slightly different.

### 6.5.2 Conclusions

The orbit of Comet Halley is chaotic (????) with a Liapounov time which we find to be  $299 \pm 62$  yr (measured over approximately the next 4 kyr). The aim of this study is to understand the origin of chaos in Halley’s orbit and its relatively short Liapounov time.

We present a model to explain the origin of chaos in few-body systems with comparable masses. We start by considering a two-body system. As is well known, in this system the difference between two solutions grows linearly, proportional to the difference in orbital fre-

quency,  $\Delta f$ , between the two solutions. When more than two bodies are present, a sequence of events (e.g. close encounters with a third body) changes  $\Delta f$ . A sequence of strong encounters produces an accumulation of power laws which resembles exponential growth.

Next we develop a model better adapted to the case of Comet Halley, where the perturbations are almost always weak, because the masses of the planets are small and very close encounters are rare. This model uses a map to describe the evolution of  $\Delta f$  in Halley's orbit. For very weak perturbations,  $\Delta f$  remains roughly constant, which results in a linear growth of perturbation or weak exponential divergence, depending on the sign of the perturbation. For somewhat stronger encounters the perturbation shows either oscillatory behaviour without secular growth (thus making Halley's orbit more stable in a sense), or exponential growth, again depending on the sign of the perturbation. Above a certain threshold in the size of the perturbation, we demonstrate that a sequence of close encounters is able to produce exponential growth, irrespective of the sign of the perturbation, with a Liapounov time of order the orbital period of Halley.

To calculate the growth of perturbations in Halley's orbit more accurately, we perform numerical N-body integrations. We find the surprising result that Venus is the dominant cause of chaos in Halley's orbit (see Fig. 6.7).